

## Optimisation of Process Parameters for Electrochemical Machining of a Curved Hole

Xurong Zhou<sup>1,2,\*</sup>, Yongfeng Jiang<sup>1,\*</sup>, Weiming Gan<sup>2,3</sup>, Yafeng He<sup>2,3</sup>, Bo Xu<sup>2,3</sup>

<sup>1</sup> College of Mechanical and Electrical Engineering, Hohai University, Changzhou 213022, P. R. China

<sup>2</sup> Department of Aeronautics and Mechanical Engineering, Changzhou Institute of Technology, Changzhou 213032, P. R. China

<sup>3</sup> Special Processing Key Laboratory of Jiangsu Province, Changzhou 213032, P. R. China

\*E-mail: [cn121314@163.com](mailto:cn121314@163.com), [jiangyf@hhuc.edu.cn](mailto:jiangyf@hhuc.edu.cn)

Received: 12 January 2021 / Accepted: 4 June 2021 / Published: 30 June 2021

---

A curved hole surface can be formed by a rotating contour tool. Owing to the shape and the material hardness, traditional cutting methods suffer from significant tool wear and poor machining efficiency. In this research we used the electrochemical machining method (ECM), in which there is no wear of tool cathode, no stress on the workpiece, high processing efficiency, and high quality machining of the curved hole is achieved. The machining gap is the key factor determining the effectiveness of ECM and the machining accuracy. In this study, numerical simulations of the ECM process were carried out. Five factors and five levels of orthogonal experiments were carried out on the main parameters affecting the machining balance gap. The optimal technological parameters consisting of the applied voltage, feed speed, initial gap, pulse duty cycle, and pulse frequency were obtained using the range analysis method. The optimized parameters were verified experimentally, and the surface roughness of the sample reached 0.613  $\mu\text{m}$ , which meets the requirements of engineering applications.

---

**Keywords:** Electrochemical Machining; Balance Gap; Orthogonal Experiment

### 1. INTRODUCTION

Curved holes are often needed in some mechanisms, where a steel ball rolls inside a curved hole. The curved hole surface is usually quenched, and because of the subsequent deformation, hole surface finishing is required after the heat treatment. The effective hardened layer depth is typically 0.8–1.2 mm, and the surface hardness is 50–65 HRC. Owing to the limitations of the contour shape, high surface hardness, and high precision required, it is problematic to use traditional cutting methods for the finishing operation of the curved hole, since the tool wear is significant, and the machining cost is too high.

Electrochemical machining (ECM) is a machining process based on Faraday's law. The process uses the principle of metal anodic dissolution in an electrolyte coupled with material removal from the

anode, which is the workpiece. The shape and dimensions of the tool cathode are a copy of the workpiece anode shape and dimensions [1, 2]. ECM has several advantages over other machining methods, such as no tool wear, no cutting forces, consistent material cutting performance, high accuracy of machining, and high machining efficiency. ECM is used in many industrial manufacturing fields such as auto parts, biomedical equipment, moulds, gears, turbine blades, and aerospace applications [3–5]. ECM is especially suitable for processing hard materials, curved surfaces, and contour-shaped surfaces of difficult to machine materials [6–8]; it offers a low cost, high efficiency, and high quality method for machining of curved holes [9]. The gap between the workpiece anode and the tool cathode directly affects the machining efficiency and surface quality. It is also the main basis for designing tool cathodes and selecting machining parameters. Furthermore, it is the main factor that influences machining accuracy. The machining gap is influenced by several factors such as the electric field, the electrolyte flow and the electrochemical parameters. The main machining parameters are conductivity, applied voltage, current density, feed rate, current efficiency and electrode potential.

The ECM machining gap has been investigated, and several methods and optimisation parameters have been studied to improve the accuracy and stability of ECM. The balance gap is defined as the optimum machining gap that offers maximum accuracy without short-circuiting. Zhang et al. [10] optimised processing parameters, such as applied voltage, and electrode feed rate, depending on the size of the balance gap to eliminate the tooth tip at the bottom of the hole and make it smooth. Chai et al. [11] studied and determined the effects of flow rate mode, applied voltage, and electrolyte concentration on the drilling efficiency, forming accuracy, and stability in the ECM of blade cooling holes. Soundarrajan et al. [12] studied the effects of electrolyte concentration, applied voltage, and duty cycle on the overcutting and processing rate for micro hole ECM. Chen et al. [13] studied the ECM of titanium alloy Ti60 blisks by means of an orthogonal experiment. The optimized electrochemical process parameters, especially the optimisation of pulse power frequency, can greatly reduce the surface roughness of blades in a Ti60 blisk. Chen et al. [14] used a masked porous cathode for ECM of micro grooves. The power supply with a frequency of 2 kHz and a pulse duty cycle of 20% was conducive to the generation of micro grooves with a low standard deviation and roughness. In addition, the processing quality was improved further by increasing the applied voltage, the depth of micro groove, and the number of reciprocating motions of the nozzle. Liu et al. [15] micro-processed 304 stainless steel tubes with a pulse electrochemical saw. They produced micro-inner-annular grooves with a depth of 340  $\mu\text{m}$  and width of 263  $\mu\text{m}$  by optimising parameters such as the dentate cathode radius, rotating speed of the rotating dentate cathode, initial gap, and feed rate. Pa [16] studied the effects of the initial gap width, electrolyte flow rate, current density, and pulse period on the ultra-finishing free-form surface. These methods provide suitable references for the ECM of curved holes. Owing to many influencing factors, complex processes, and difficult process control, further research is still needed to improve the accuracy and process stability of the ECM of curved holes.

To improve the quality of ECM, several researchers have used orthogonal tests to optimise multi-objective parameters. Prayogo et al. [17] optimised processing parameters using the Taguchi  $L_9$  orthogonal array method and determined the effects of electrolyte concentration, voltage, and machining gap width on the material removal rate. Tang et al. [18] analysed the influence of voltage and feed speed on material removal rate, side clearance, and surface roughness by orthogonal array testing and Grey

relational analysis and obtained the optimal parameters. Pawar et al. [19] used the Taguchi L<sub>27</sub> orthogonal array method and Gray correlation analysis to input parameters (electrolyte concentration, applied voltage, and tool rotation) into the ECM of silicon carbide. They determined that electrolyte concentration is the main factor affecting the diameter and depth of machined holes. In the current study, the ECM curved hole was used as the research object. The design of the side-flow channel was studied and numerical simulation and ECM testing were conducted. A five-level orthogonal test was designed for the applied voltage, feed speed, initial gap, pulse duty cycle, and pulse frequency. The range analysis of the test results was conducted to determine the degree of influence of the process parameters on the machining gap, and parameter optimisation was carried out. Finally, the process parameters were tested to confirm the improvement of the test results.

## 2. NUMERICAL SIMULATION OF ECM OF THE CURVED HOLE

### 2.1. Geometric model of ECM of the curved hole

In ECM, the workpiece is the anode and the curved hole tool is the cathode, connected to the negative and positive poles of the power supply, respectively. As shown in Fig. 1. the anode is fixed to the worktable, and the cathode is installed on the spindle of the machine tool, which can move up and down the spindle. The electrolyte as the conductive medium flows at a high speed through the machining gap formed by the cathode and the anode. When the cathode moves rapidly towards the anode, the electrochemical reaction and anodic dissolution of the anode occurs under the action of the DC stabilised voltage pulse power supply, and the material making up the anode is dissolved. With the continuous flow of the electrolyte, the anode material is removed and electrolytic products are produced, gradually forming the curved hole.

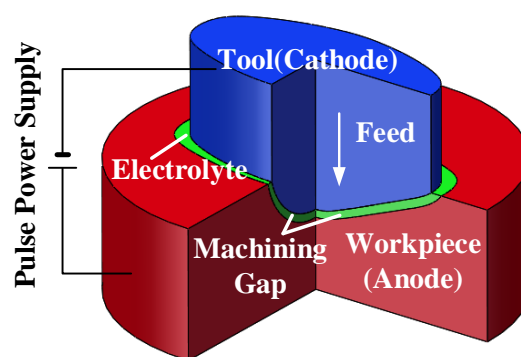


**Figure 1.** Schematic of ECM of the curved hole

The machining gap is the most important factor of ECM when determining the machining accuracy. When the machining process reaches balance, there is a constant gap between the cathode and the anode, which is called the balance gap  $\Delta_b$ . If the balance gap is too large, the machining accuracy is reduced; if the balance gap is too small, there is a risk of a short circuit. In ECM experiments, the balance

gap is an important basis for cathode and anode shape design. The balance gap of pulsed ECM is calculated using equation (1),

$$\Delta_b = \eta \omega \frac{k U_R}{v} \quad (1)$$

where  $\eta$  is the current efficiency,  $\omega$  is the volume electrochemical equivalent,  $k$  is the electrolyte conductivity,  $U_R$  is the voltage drop between the cathode and anode, and  $v$  is the feed rate of the cathode. The current efficiency  $\eta$  depends on the anode material, electrolyte, and current density. The volume electrochemical equivalent,  $\omega$  is also determined by the anode material. The electrolyte conductivity  $k$  is related to the initial gap and electrolyte temperature.  $kU_R/v$  is the processing condition, which is determined by the applied voltage, cathode feed rate, and electrolyte composition. In addition, the applied voltage is dependent on the power frequency and duty cycle.

## 2.2. Design of the side-flow channel with the curved hole

Figure 2 shows the side-flow channel model of a curved hole. Because of the geometric shape of the curved hole, the side flow type of electrolyte flow is needed in ECM; that is, the electrolyte flows from one side of the machining gap, through the machining gap and out the other side. The flow direction of the electrolyte should ensure the shortest flow path and a uniform flow field, therefore, one long side of the curved hole is selected for the electrolyte to flow in and the opposite long side to flow out.

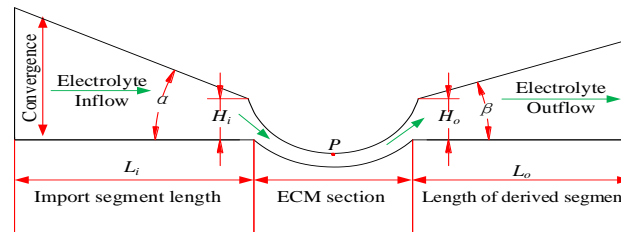


**Figure 2.** Side-flow channel model of the curved hole

The flow pattern of the electrolyte in the machining gap affects the stability of the ECM process. The function of the electrolyte is to establish an electrochemical reaction electrode system and wash away electrolytic products together with the heat generated by the electrochemical reaction. A stable flow field improves the precision and stability of the ECM of a curved hole. To ensure that the flow field on the machining surface of the curved hole is uniform, a correct length of the diversion section [20] must be established before the machining gap inlet. In addition, a similar length of the diversion section must be established after the machining outlet. This ensures that the full length of the gap is in a turbulent state, and no streamline intersection occurs to avoid the formation of cavitation and prevent electrolytic separation phenomena. Therefore, the electrolyte channel needs to be designed for the side flow. As shown in Fig. 2, there is a guide section of length  $L_i$  and height  $H_i$  in front of the machining inlet. It converges into the machining gap at an angle of  $\alpha$  to improve the stability of the flow field; similarly, there is a guide section of length  $L_o$  and height  $H_o$  at the outlet, and the electrolyte flows out from the

machining gap expanding at an angle of  $\beta$ . After numerical simulation, six kinds of parameters of the side flow channel were identified.

### 2.3. Numerical simulation

In the numerical simulation, the mass concentration of the  $\text{NaNO}_3$  electrolyte solution was 10%, the electrolyte temperature was  $27\text{ }^\circ\text{C}$ , the electrolyte inlet pressure was 0.8 MPa, the outlet pressure was 0.2 MPa, the initial gap was 0.3 mm, and the inter-electrode voltage was set to 18 V. The six parameters ( $L_i$ ,  $H_i$ ,  $\alpha$ ,  $L_o$ ,  $H_o$ , and  $\beta$ ) defining the side flow channel were pre-set with three values each, and the distributions of the electric field, flow field, and bubble rate were calculated by COMSOL Multiphysics software. By comparing the numerical results at point P (as shown in Fig. 2), the parameters favourable for ECM were selected. The optimal settings determined were  $L_i = 27\text{ mm}$ ,  $H_i = 3\text{ mm}$ , the angle  $\alpha = 18^\circ$ ,  $L_o = 27\text{ mm}$ ,  $H_o = 3\text{ mm}$ , and the angle  $\beta = 15^\circ$ . The distributions of the electric field, flow field, and bubble rate of the curved hole were obtained by numerical simulation using the six parameters of the side flow channel.

#### 2.3.1. Electric field distribution

The current density distribution of the curved hole obtained was as shown in Fig. 3. The electrolyte was injected from the inlet of the guide section, flowed through the inlet, bottom and outlet of the machining gap, and finally flowed out from the outlet of the guide section. Figure 3 shows that the current density gradually increased from Section A to B, and decreased from Section B to C; it reached  $5.52 \times 10^4\text{ A/m}^2$  at the lowest point P on the cathode surface in section B.

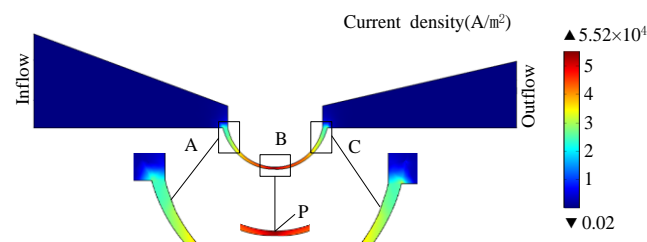


**Figure 3.** Current density distribution of the curved hole

#### 2.3.2. Flow field distribution

The flow field distributions of the curved hole consisting of the pressure and velocity distributions, are shown in Figs. 4 and 5. The pressure in the machining gap determined the speed of the electrolyte passing through the machining gap. In addition, the electrolyte had to overcome the viscous friction resistance of the electrolyte in the machining gap. Owing to the increase of the flow velocity of

the electrolyte, the flow velocity in the channel slowed. This can cause the electrolyte to vaporize, so it is important to attend to any change of flow pressure.

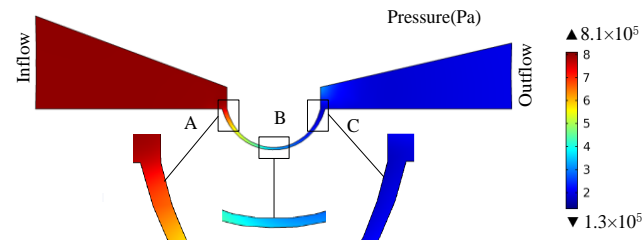


**Figure 4.** Pressure distribution of the curved hole

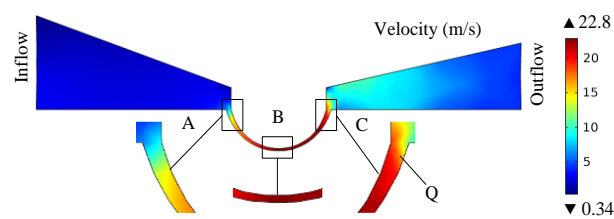


**Figure 5.** Velocity distribution of the curved hole

Figure 4 shows the pressure distribution for the whole flow channel when the inlet electrolyte pressure was 0.8 MPa. From the inlet to the bottom of the machining gap to the outlet, the pressure gradually decreased. Figure 5 shows the electrolyte flow velocity distribution at the inlet. From the inlet to the bottom of the processing gap, the flow velocity gradually increased, reaching a maximum of 22.8 m/s. As the outlet gap of the processing area gradually increased, the flow velocity at the outlet Q point started to decrease. There was no electrolyte vortex area because the velocity of the machining area in the channel increased first and then decreased gradually, therefore there was no sudden change in the velocity in the machining area. This ensured that high quality of the ECM was maintained and short-circuits and combustion between the cathode and anode were avoided.

### 2.3.3. Distribution of bubble ratios

Bubbles are the main factor affecting the uniformity of the electric field distribution. During the ECM of a curved hole, numerous bubbles were generated in the machining area by the electrochemical reactions. Some bubbles were carried out of the machining area with the electrolyte and electrolytic products, and some bubbles were destroyed by the impact of the electrolyte, however some bubbles remained in the machining area. Figure 6 shows the distribution of bubble ratios in the ECM of the curved hole. This figure shows that the bubbles at the inflow (A section) to the bottom (B section) of the machining gap were taken away by the electrolyte. The bubbles gradually increased from the bottom (B section) to the outflow (C section) and gathered along the flow direction. The number of bubbles at point

Q of C section was the highest, when the bubble ratio reached 0.15. As the number of bubbles increased, the conductivity decreased, and the dissolution rate slowed down.

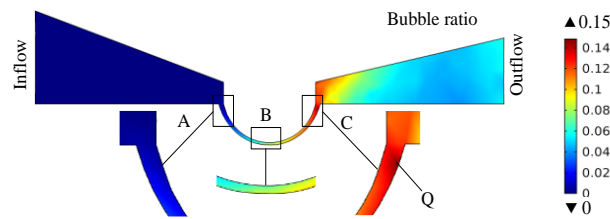


Figure 6. Bubble ratio distribution of the curved hole

### 3. EXPERIMENTAL TEST SCHEME AND CONDITIONS

#### 3.1. Test equipment

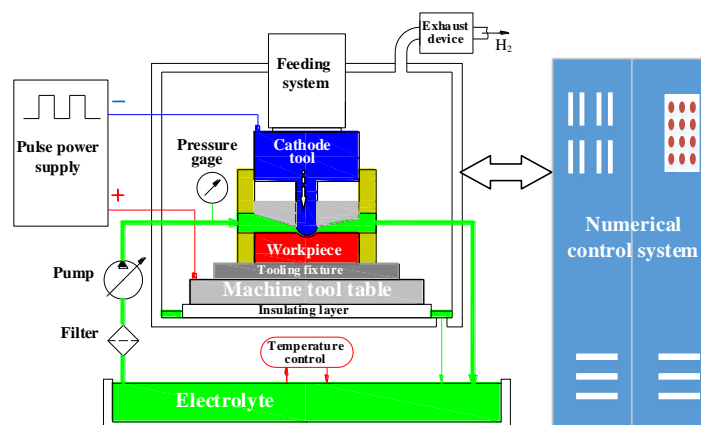
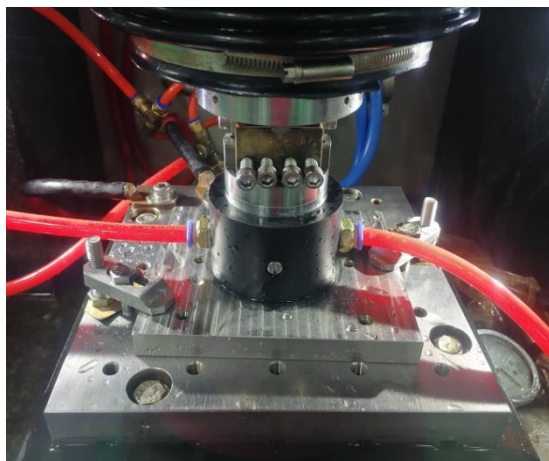
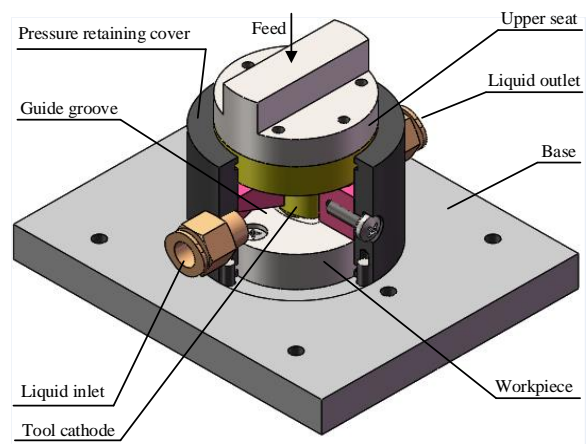


Figure 7. The ECM test system for the curved hole

Figure 7 shows the ECM test system for the curved hole, which comprises the ECM machine tool, the control system, the electrolyte filtration system, the workpiece fixture, and a pulse power supply. The feed system is installed on the spindle of the machine tool. The tool cathode is connected to the feed system and provides linear reciprocating motion along the z-axis. The workpiece is fixed to the fixture. Under the action of the pump, the electrolyte flows through the inlet of the guide section, through the machining gap, and out through the outlet of the guide section. The temperature control system regulates the temperature of the electrolyte, and the workpiece dissolves under electrochemical action, finally completing the ECM process.



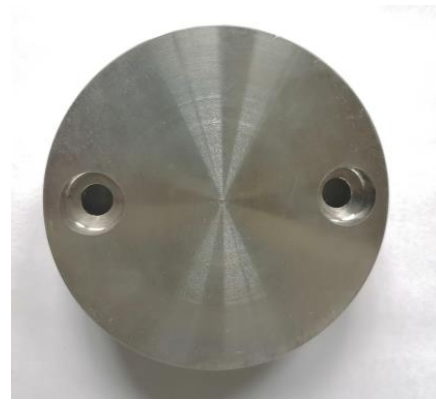
(a) Actual clamp



(b) Clamp schematic



(c) Tool cathode



(d) Workpiece blank

**Figure 8.** ECM test fixture

### 3.2. Test fixture

The actual clamping device and the clamp schematic drawing are shown in Figs. 8(a) and 8(b), respectively. The clamping device includes the upper seat, base, and pressure retaining cover. The upper seat is pulled onto the machine tool spindle through a U-shaped groove on the machine tool spindle, and the tool cathode (as shown in Fig. 8(c)) is fixed to the upper seat by means of screws. The tool cathode can be disassembled to be replaced after any short-circuit burn in the ECM process. The overall dimension of the workpiece blank, shown in Fig. 8(d), is  $\phi 68 \times 20$  mm. The workpiece is fixed on the fixture base by means of screws through the base, making it easy to replace after processing. The pressure retaining cover is fixed to the base, to cover the tool cathode and workpiece blank. There are two guide grooves in the front and back of the processing area between the cathode tool and the workpiece blank. The electrolyte flows in through the liquid inlet of the fixture, enters the processing area through the guide groove, then flows through another guide groove, and finally flows out through the liquid outlet.

### 3.3. Orthogonal test design

The test parameters were consistent with the numerical simulation parameters. The conductivity  $k$  of  $\text{NaNO}_3$  solution with 10% mass fraction was  $7.82 \times 10^{-2} \Omega^{-1} \cdot \text{cm}^{-1}$ . The electrolyte temperature was set at  $27^\circ\text{C}$  and the temperature control system was maintained in the range of  $27 \pm 0.5^\circ\text{C}$ . The inlet pressure of the electrolyte was set at 0.8 MPa, and the outlet pressure was set at 0.2 MPa. The applied voltage was set at 16–24 V, the feed speed was set at 0.4–0.8 mm/min, the pulse power frequency and duty cycle were 100–500 Hz and 0.7–0.9 respectively, and the initial gap was set at 0.2–0.6 mm. In this study, the applied voltage (AV), feed speed (FS), duty cycle (DC), pulse frequency (PF,) and initial gap (IG) were used as test processing parameters. Five levels of each factor were selected to design the  $L_{25}$  ( $5^5$ ) orthogonal test. Table 1 shows the factors and levels of the orthogonal test.

**Table 1.** The orthogonal test parameters

| Levels | Factor                   |                          |                 |                            |                       |
|--------|--------------------------|--------------------------|-----------------|----------------------------|-----------------------|
|        | Applied voltage (V)<br>A | Feed speed (mm/min)<br>B | Duty cycle<br>C | Pulse frequency (kHz)<br>D | Initial gap (mm)<br>E |
| 1      | 16                       | 0.4                      | 0.70            | 0.1                        | 0.2                   |
| 2      | 18                       | 0.5                      | 0.75            | 0.2                        | 0.3                   |
| 3      | 20                       | 0.6                      | 0.80            | 0.3                        | 0.4                   |
| 4      | 22                       | 0.7                      | 0.85            | 0.4                        | 0.5                   |
| 5      | 24                       | 0.8                      | 0.90            | 0.5                        | 0.6                   |

## 4. RESULTS AND DISCUSSION

### 4.1. Results

The five factors and five-level orthogonal test scheme and test results are shown in Table 2, and the processed samples are shown in Fig. 9, with a total of 25 groups. The sum of the yield and the average yield of each factor were calculated. The sum of the yield  $I_j$ ,  $II_j$ ,  $III_j$ ,  $IV_j$ , and  $V_j$  and the average yield  $Av_{1j}$ ,  $Av_{2j}$ ,  $Av_{3j}$ ,  $Av_{4j}$ , and  $Av_{5j}$  are shown in Table 3, where  $I_j$  is the sum of the data corresponding to the first level of column  $j$ .  $Av_{1j}$  is the average value of the sum of data corresponding to the first level of column  $j$ , and the rest follow similarly.  $R$  in Table 3 is the range, which is calculated from equation (2), and is the difference between the maximum and minimum average yield for the same factor.

$$R = Av_{ijmax} - Av_{ijmin} \quad (2)$$

From the test results and range analysis shown in Table 3, the following conclusions can be drawn:

**Table 2.** Five factors and five-level orthogonal test scheme and results

| No. | AV (A) | FS (B) | DC (C) | PF (D) | IG (E) | Balance Gap (mm) |
|-----|--------|--------|--------|--------|--------|------------------|
| 1   | 1      | 1      | 1      | 1      | 1      | 0.153            |
| 2   | 1      | 2      | 2      | 2      | 2      | 0.164            |
| 3   | 1      | 3      | 3      | 3      | 3      | 0.156            |
| 4   | 1      | 4      | 4      | 4      | 4      | 0.162            |
| 5   | 1      | 5      | 5      | 5      | 5      | 0.124            |
| 6   | 2      | 1      | 2      | 3      | 4      | 0.183            |
| 7   | 2      | 2      | 3      | 4      | 5      | 0.197            |
| 8   | 2      | 3      | 4      | 5      | 1      | 0.185            |
| 9   | 2      | 4      | 5      | 1      | 2      | 0.177            |
| 10  | 2      | 5      | 1      | 2      | 3      | 0.169            |
| 11  | 3      | 1      | 3      | 5      | 2      | 0.228            |
| 12  | 3      | 2      | 4      | 1      | 3      | 0.229            |
| 13  | 3      | 3      | 5      | 2      | 4      | 0.211            |
| 14  | 3      | 4      | 1      | 3      | 5      | 0.202            |
| 15  | 3      | 5      | 2      | 4      | 1      | 0.193            |
| 16  | 4      | 1      | 4      | 2      | 5      | 0.258            |
| 17  | 4      | 2      | 5      | 3      | 1      | 0.263            |
| 18  | 4      | 3      | 1      | 4      | 2      | 0.243            |
| 19  | 4      | 4      | 2      | 5      | 3      | 0.233            |
| 20  | 4      | 5      | 3      | 1      | 4      | 0.224            |
| 21  | 5      | 1      | 5      | 4      | 3      | 0.308            |
| 22  | 5      | 2      | 1      | 5      | 4      | 0.296            |
| 23  | 5      | 3      | 2      | 1      | 5      | 0.275            |
| 24  | 5      | 4      | 3      | 2      | 1      | 0.261            |
| 25  | 5      | 5      | 4      | 3      | 2      | 0.255            |



(a) No. 1, 3, 5, ..., 25



(b) No. 2, 4, 6, ..., 24

**Figure 9.** Processing sample

(1) According to the magnitude of the range, the order of influence of each factor on the index was (from highest to lowest): AV → FS → PF → IG → DC.

(2) For the balance gap, the smaller the value, the better the result. Therefore, the smallest one was selected. The average values of  $Av_{1j}$ ,  $Av_{2j}$ ,  $Av_{3j}$ ,  $Av_{4j}$ , and  $Av_{5j}$  of each factor under five levels were compared from the test results. The parameter value corresponding to the minimum average was selected. The best level combination was  $A_1B_5C_2D_1E_1$ , that is, the applied voltage is 16 V, the feed speed is 0.8 mm/s, the duty cycle is 0.75, the pulse frequency is 0.1 kHz, and the initial gap is 0.2 mm, as shown in Table 4.

**Table 3.** Test analysis results

| Parameters                              | A      | B      | C      | D      | E      |
|---|--------|--------|--------|--------|--------|
| $I_j$                                   | 0.759  | 1.130  | 1.063  | 1.058  | 1.055  |
| $II_j$                                  | 0.911  | 1.149  | 1.048  | 1.063  | 1.067  |
| $III_j$                                 | 1.063  | 1.070  | 1.066  | 1.059  | 1.095  |
| $IV_j$                                  | 1.221  | 1.035  | 1.054  | 1.103  | 1.076  |
| $V_j$                                   | 1.395  | 0.965  | 1.079  | 1.066  | 1.056  |
| $Av_{1j}$                               | 0.1518 | 0.2260 | 0.2126 | 0.2116 | 0.2110 |
| $Av_{2j}$                               | 0.1822 | 0.2298 | 0.2096 | 0.2126 | 0.2134 |
| $Av_{3j}$                               | 0.2126 | 0.2140 | 0.2132 | 0.2118 | 0.2190 |
| $Av_{4j}$                               | 0.2442 | 0.2070 | 0.2108 | 0.2206 | 0.2152 |
| $Av_{5j}$                               | 0.2790 | 0.1930 | 0.2158 | 0.2132 | 0.2112 |
| R                                       | 0.1272 | 0.0368 | 0.0062 | 0.0090 | 0.0080 |
| Order of influence: $A > B > D > E > C$ |        |        |        |        |        |
| Optimum combination: $A_1B_5C_2D_1E_1$  |        |        |        |        |        |

**Table 4.** Optimal level combination

| Applied voltage (A) | Feed speed (B) | Duty cycle (C) | Pulse frequency (D) | Initial gap (E) |
|---------------------|----------------|----------------|---------------------|-----------------|
| 16 V                | 0.8 mm/min     | 0.75           | 0.1 kHz             | 0.2 mm          |

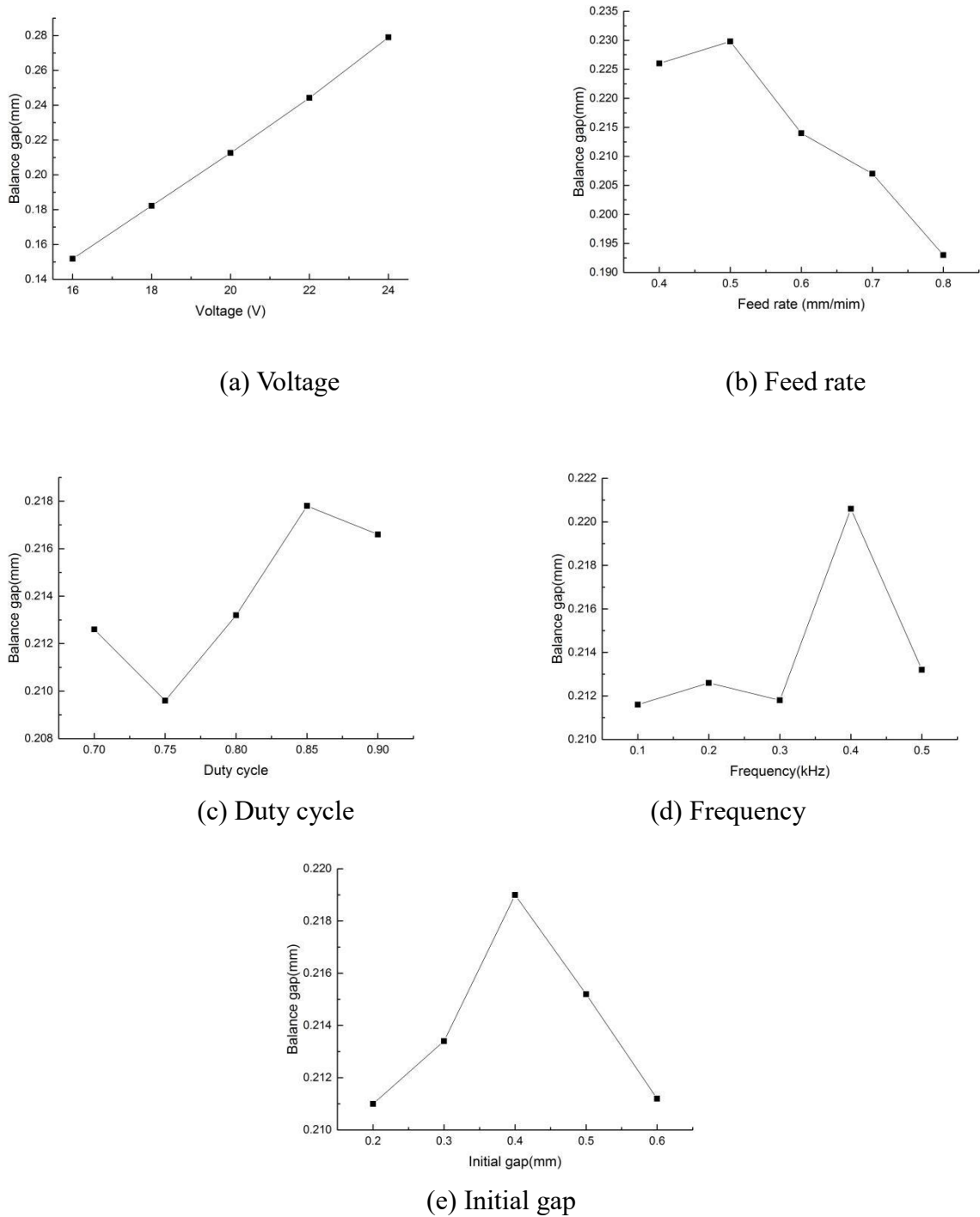


**Figure 10.** Influence of machining parameters on balance gap

#### 4.2 Discussion

Table 2 shows the effects of the processing parameters (applied voltage, feed speed, duty cycle, pulse frequency, and initial gap) on the balance gap, as shown graphically in Fig. 10. According to Faraday's law, the rate of material removal is directly proportional to the current density.

#### 4.2.1. Influence of applied voltage on the balance gap

The applied voltage is a key process parameter that establishes the electric field between the electrodes in an ECM process. In addition, it ensures the continuity of the ECM process, and maintains the current density.

Table 3 shows that the applied voltage has the greatest influence on the balance gap. Figure 10(a) shows that with other ECM process conditions fixed, when the applied voltage increases from 16 to 24 V, the balance gap increased from 152 to 279  $\mu\text{m}$ , an increase of 83.6%. The balance gap had a linear relationship with the applied voltage, which conformed to the balance gap equation (1) above. When the applied voltage increased, the current density of the cathode and anode of the curved hole also increased, while the feed speed remained unchanged. In addition, the electrolytic reaction became more intense, which led to a higher dissolution rate of the metal at the anode, and an increase of the balance gap.

Zhang et al. [10] found that when drilling with hollow tube electrolysis, the balance gap was small when drilling with low voltage and a high feed rate, however, when drilling with high voltage and a low feed rate, the balance gap was bigger. Chai et al. [11] found that the unilateral gap of the cooling hole increased when the applied voltage increased, because the increase led to a higher current density between tube tool and the cooling hole, which caused a higher dissolution rate of the workpiece materials and a larger unilateral gap. Chen et al. [13] studied the ECM of titanium alloy Ti60 blisks, and found that with the increase of applied voltage, the electrochemical reaction became more intense, and numerous electrolytic products collected in the machining area, making the surface rougher. R. Wüthrich et al. [21] concluded that the material removal rates depend on a large number of parameters, such as material to be processed, electrolyte used, applied voltage and temperature.

#### 4.2.2 Influence of feed rate on the balance gap

The feed rate is the speed rate of the cathode. Table 3 shows that the feed rate had a significant influence on the balance gap. When the feed speed was 0.8 mm/min, the balance gap was the least. Figure 10(b) shows that with the increase of feed rate, the balance gap first increased from 226 to 230  $\mu\text{m}$  and then decreased to 193  $\mu\text{m}$ , and the overall decrease was 14.6%. The balance gap was inversely proportional to the feed rate, which was in line with the balance gap equation (1). The main reason for this was that with the increase of feed rate, the current density also increased, which accelerated the electrolytic corrosion of the anode materials. The feed rate was faster than the material dissolution rate, further reducing the gap between the cathode and anode. If the feed rate was too high, it caused short circuits during the machining process.

Anasane et al. [22] also found in the ECM of titanium-based through-holes that the gap between the electrodes was further reduced when the feed rate of microtools was faster than the dissolution rate of materials. Liu et al. [15] studied the pulsed electrochemical sawing of annular micro grooves in metal tubes and found that the balance gap decreased with the increase of feed rate. However, when the machining gap was too small, the electrochemical reaction became very violent, and unexpected discharges and short circuits occurred.

#### 4.2.3 Influence of duty cycle rate on the balance gap

The duty cycle is an important parameter for a pulse power supply. Duty cycle refers to the proportion of time that the power is on relative to the total time in a pulse cycle. Figure 10(c) shows that when the duty cycle was 0.75, the balance gap was smallest. As the duty cycle increased from 0.7 to 0.9, the balance gap fluctuated from 210 to 218  $\mu\text{m}$ . The increase of duty cycle increased the rising edge time in a single pulse, resulting in an increase in the current density per unit of time. This resulted in more materials dissolving at the anode, thus forming a larger balance gap.

Chen et al. [14] found that when the pulse duty cycle increased, the pulse conduction time also increased, and the pulse cut-off time shortened. The electrolytic products and bubbles that could not be discharged in time slowed the deep dissolution of the material, which made the microcell profile and roughness worse. Chen et al. [13] also found that when the power duty cycle was low, there was enough time to remove the electrolytic products, the electrochemical dissolution was easier, and the surface was smoother. Anasane et al. [21] reported that when conducting ECM of titanium through-holes, when the duty cycle increased, the amount of sludge produced also increased. The available closing time was not enough to flush away the sludge produced, and less fresh electrolyte was available in the narrow processing area. The surface roughness increased with the increase of duty cycle.

#### 4.2.4 Influence of power frequency on the balance gap

The power frequency is another important parameter of the pulse power supply. Figure 10(d) shows that the balance gap is smallest at a power frequency of 0.1 kHz. When the frequency increased to 0.5 kHz, the balance gap fluctuated between 212 and 221  $\mu\text{m}$ . The influence of power frequency on the balance gap was not an important factor. The advantage of the pulse power supply was intermittent corrosion during the ECM process. The intermittent oscillation accelerated the renewal of electrolyte. With the increase of pulse power supply frequency, the frequency and intensity of the inter-electrode pulsating pressure wave increased, and the stirring effect on the inter-electrode electrolyte was stronger so that the electrolytic corrosion products were flushed away more timeously. In this experiment, the frequency ranges from 0.2 to 0.3 kHz and from 0.4 to 0.5 kHz were consistent with this rule.

Chen et al. [14] found that the frequency of the pulse power supply was too low, and there was not enough time to remove the electrolytic products, which led to roughness on the surface of the workpiece. When the frequency of the power supply exceeded a certain value, the electrolytic products washed away in the pulse interval, and the roughness of the surface of the workpiece improved. Anasane et al. [21] also found that increasing the pulse frequency reduced the surface roughness.

#### 4.2.5 Influence of the initial gap on the balance gap

The initial gap is the distance between the cathode and anode before the start of machining, and it is also one of the factors affecting the balance gap. Figure 10(e) shows that with the increase of the initial gap from 0.2 to 0.8 mm, the balance gap first increased from 211 to 219  $\mu\text{m}$ , and then decreased

to 212  $\mu\text{m}$ , and the minimum balance gap occurred with an initial gap of 0.2 mm. When the initial gap was between 0.2 and 0.4 mm, the increase of the initial gap enabled more of the electrolytic products to be contained in the machining gap. At the same time, it was easy for the fresh electrolyte to enter the machining gap. Under the action of a pulse current, the discharge speed of the electrolytic products was accelerated, which accelerated the flow of electrolyte from the anode to the cathode and increased the rate of the electrolytic products production. The balance gap increased with the discharge of the material and the dissolution of the anode. When the initial gap increased from 0.4 to 0.6 mm, the current density, the material removal rate, and the balance gap decreased.

Liu et al. [15] reported that when the initial gap increased, the current density decreased, and the annular micro-grooves' removal in the metal tube was reduced. When the initial gap decreased, the renewal of electrolyte in the machining gap was limited, which led to the limitation of micro-grooves' discharge.

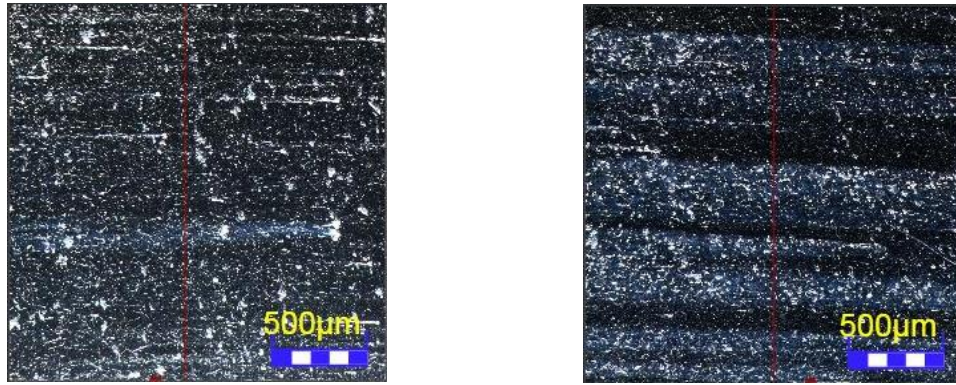
#### 4.3. Experimental verification after optimisation of parameters

The optimised combination,  $A_1B_5C_2D_1E_1$ , was not one of the 25 orthogonal experiments. The optimised parameters were as follows: an AV of 16 V, a feed rate of 0.8 mm/s, a duty cycle of 0.75, a pulse frequency of 0.1 khz, and an initial gap of 0.2 mm. With the other processing conditions unchanged, the ECM process parameters were adjusted to reach the optimal combination to carry out the verification test. The balance gap of the workpiece was 0.092 mm, the surface roughness was 0.613  $\mu\text{m}$ , which was 25.8% shorter than the balance gap of 0.124 mm in the fifth group test, and the surface roughness was reduced by 7.8% to 0.665  $\mu\text{m}$ . Fig. 9 (a) shows the sample processed using the combination of the optimal process parameters, and (b) shows the fifth group of test samples.



(a) Original drawing of test sample after optimisation of parameters (b) Original drawing of group 5 test sample

**Figure 9.** Comparison of original sample drawings



(a) Surface morphology and roughness of optimized combination test (b) Surface morphology and roughness of group 5 test

**Figure 10.** Comparison of the morphology of SEM specimens

Fig. 10 (a) shows the morphology of the sample processed using the combination of the optimal process parameters and Fig. 10 (b) shows the sample processed using the combination of the fifth group of test parameters—which were taken in the range of  $1994 \mu\text{m} \times 1994 \mu\text{m}$ , respectively. The surface smoothness of the specimens processed using the optimised parameters was higher than that of the specimens processed using the parameters of the fifth group.

## 5. CONCLUSIONS

Using ECM of a curved hole as our research object, an orthogonal experiment involving five factors and five levels was carried out, and the following conclusions were reached:

- (1) Side-flow channel pulse ECM is suitable for ECM of a curved hole.
- (2) Of the five process parameters examined, the applied voltage and the feed speed were the most influential factors affecting the balance gap. The balance gap increased with the increase in applied voltage, and decreased with an increase of feed speed.
- (3) The five most important parameters affecting the balance gap were, in order of decreasing influence: applied voltage, feed speed, pulse frequency, initial gap, and duty cycle.
- (4) The optimal settings for the parameters were: applied voltage = 16 V, feed speed = 0.8 mm/s, duty cycle = 0.75, pulse frequency = 0.1 kHz, and initial gap = 0.2 mm.

## ACKNOWLEDGEMENTS

This work was supported by Key R&D Projects of JiangSu Province (BE2018067) and The Natural Science Foundation of the Jiangsu Higher Education Institutions of China (19KJA430005).

## References

1. K.P. Rajurkar, D. Zhu, J.A. McGeough, J. Kozak, A. De Silva, *Annals of the CIRP*, 48(1999)567.

2. Y. Liu, N.S. Qu, *Int. J. Mech. Sci.*, 169(2020)105333.
3. K.P. Rajurkar, H. Hadidi, J. Pariti, and G.C. Reddy, *Procedia Manuf.*, 7 (2016) 714.
4. Z Pandilov, *IOP Conf. Ser.: Mater. Sci. Eng.*, 329(2018)012014.
5. Y.L. Chen, M. Fang, L.J. Jiang, *Int. J. Adv. Manuf. Technol.*, 91 (2017) 2455.
6. D. Zhu, L.G. Yu, J.B. Zhao, J. Liu, Z.Y. Xu, *Int. J. Adv. Manuf. Tech.*, 102( 2019)559.
7. S. Ayyappan and N. Vengatajalapathi, *Adv. Unconven. Mach. Composit.*, 21(2020)255.
8. R. Raja and Sabitha Jannet, *Adv. Unconven. Mach. Composit.*, 48(2020)583.
9. F. Klocke, M. Zeis, A. Klink, D. Veselovac, *CIRP J. Manuf. Sci. Technol.*,6(2013)198.
10. Y.H. Zhang, N.S. Qu, X.L. Fang, X.D. Wang, *J. Manuf. Processes*, 37(2019)488.
11. M.X. Chai, Z.Y. Li, H.J. Yan, and X.Y. Sun, *Adv. Mater. Sci. Eng.*, 2019(2019)1.
12. M. Soundarrajan, and R. Thanigaivelan, *Mater. Manuf. Processes*, 35(2020)755.
13. X.Z. Chen, Z.Y. Xu, Z.D. Fang, D. Zhu, *Chin. J. Aeronaut.*, 29 (2016) 274.
14. X.L. Chen, G.C. Fan, C.H. Lin, B.Y. Dong, Z.N. Guo, X.L. Fang, N.S. Qu, *J. Mater. Process. Technol.*, 276(2020)116406.
15. G.X. Liu, Y.J. Zhang, S.Z. Jiang, J.W. Liu, G.K. Gyimah, H.P. Luo, *Int. J. Mach. Tools Manuf.*, 102(2016)22.
16. P.S. Pa, *J. Vac. Sci. Technol., B*, 27(2009)1221.
17. Galang Sandy Prayogo and Nuraini Lusi, *IOP Conf. Ser.: Mater. Sci. Eng.*, 494(2019)012055.
18. L. Tang, S. Yang, *Int. J. Adv. Manuf. Tech.*, 67(2013)2909.
19. Pravin Pawar, Amaresh Kumar, Raj Ballav, *Ann. Chim-Sci. Mat.*, 44(2020)239.
20. Y.F. He, J.S. Zhao, H.X. Xiao, W.Z. Lu, W.M. Gan, F.H. Yin, Z.W. Yang, *Int. J. Electrochem. Sci.*, 13 (2018) 5736.
21. R. Wüthrich, V. Fascio, *Int. J. Mach. Tools Manuf.*, 45(2005)1095.
22. Sandip S. Anasane, B. Bhattacharyya, *Int. J. Adv. Manuf. Technol.*, 105(2019)4585.